

Reaction $^{16}\text{O}(\pi^+, pp)^{14}\text{N}$ at 60 MeV: Testing the quasi-deuteron mechanism

M. Gouweloos and M. Thies

Natuurkundig Laboratorium der Vrije Universiteit, 1007 MC Amsterdam, The Netherlands

(Received 28 August 1986)

A recently proposed phenomenological version of the quasi-deuteron mechanism for pion absorption is applied to low energy pions in flight. We analyze the 60 MeV high resolution data of the reaction $^{16}\text{O}(\pi^+, pp)^{14}\text{N}$. The distorted wave calculations are successful for the transition to the 3.9 MeV 1^+ state, but fail to explain triple differential cross sections for the transition to the ground state. The strongly anisotropic recoil angle distributions for both states are well accounted for by distortion and polarization effects, the latter being characteristic for transitions with $L \neq 0$. Predictions for 2^+ and 3^+ states are given which should allow us to verify our tentative explanation of the recoil angle dependence.

I. INTRODUCTION

The mechanism of pion absorption in nuclei is still poorly understood.¹ Experimental efforts trying to change this situation fall roughly into two categories: detailed studies of the two-nucleon absorption mechanism on one hand, and attempts to identify signatures of many-body absorption mechanisms on the other. Here, we focus on the first class of measurements, the prototype of which is the (π, NN) coincidence reaction.²⁻⁷ Only very recently have sufficient statistics and energy resolution been obtained to allow the investigation of transitions to definite final nuclear states.^{8,9} This opens the possibility for a quantitative exploration of the "quasi-deuteron mechanism" (QDM) in complex nuclei. In a previous paper¹⁰ (hereafter referred to as I), we have advocated the use of a phenomenological πNN absorption operator at low energies, and presented first results for stopped pions. In the present study, we apply the same strategy to analyze the recent 60 MeV in flight absorption data on ^{16}O from LAMPF.⁸

Before turning to these new calculations, it may be worthwhile to recapitulate some results of our preceding work (I). Briefly, our approach consists of constructing a phenomenological $\pi NN \rightarrow NN$ transition operator with free strength parameters characterizing its partial wave content. This operator is then imbedded in a standard distorted wave impulse approximation (DWIA) scheme, and hopefully allows the correlation of a large variety of data in an economic and physically motivated way. The purely phenomenological approach may suggest a great flexibility which can accommodate almost everything, at the cost of having very little predictive power. However, in practice, this is not the case: The mere assumption that absorption proceeds via the QDM already yields very strong correlations among different observables. For stopped pions, for instance, we found that most distributions are governed by the recoil momentum distribution, rather than the dynamics of the elementary absorption process. In such a case, discrepancies with the data cannot be reconciled by exploiting the freedom contained in the $\pi NN \rightarrow NN$ transition operator, but indicate nuclear

structure problems or a breakdown of the QDM as such.

In the (π^+, pp) coincidence measurement on ^{16}O at 60 MeV, two distinct transitions leading to the ground state and 3.9 MeV 1^+ state of ^{14}N were studied in detail.⁸ The data show two unexpected qualitative features: The recoil momentum distribution for the g.s. transition exhibits a maximum at $P_R = 0$ in conflict with its generally assumed $L=2$ character, and there is a very strong, state-dependent variation with the direction of the recoil momentum vector. In its simplest form, the QDM predicts no dependence on this variable at all. These puzzling observations are the main motivation for the present study.

The plan of the paper is as follows. Section II contains the basic elements of the QDM for pions in flight, including an analytically soluble simple model which has already proven instructive in the stopped pion case (I). In Sec. III we compare this schematic model with the ^{16}O data at 60 MeV, concentrating on the qualitative aspects. Section IV is devoted to DWIA calculations and detailed comparisons between measured and calculated triple differential cross sections. It is followed by a brief conclusion.

II. THE QUASI-DEUTERON MECHANISM FOR PION ABSORPTION IN FLIGHT

The aim of this section is twofold: First, we recall the main features of our phenomenological π -two-nucleon absorption operator and collect some information on the inherent strength parameters. Secondly, we discuss a schematic model for pion absorption on a pair in a complex nucleus, which exhibits the dynamical information content of various experimental observables. This qualitative discussion will serve as the framework for our analysis of the experimental data later on. Since the formalism developed here is quite similar to the stopped pion case (I), we shall be less explicit, concentrating on the novel aspects for pions in flight.

At low pion energies ($T_\pi < 100$ MeV), six partial wave amplitudes are needed in order to specify pion absorption on all possible NN pairs in relative s states. As a re-

minder, we list in Table I the relevant quantum numbers. Following paper I, we write the t -matrix element for the reaction $\pi(\text{NN})_{\text{bound}} \rightarrow \text{NN}$ in a way which emphasizes the spin structure:

$$\langle \mathbf{q} | t_{\text{abs}} | \boldsymbol{\kappa} \rangle = \sum_{S'} \dot{\mathbf{S}}(S', S) \cdot \mathbf{V}(S', S). \quad (2.1)$$

Here, $\boldsymbol{\kappa}$ and \mathbf{q} are the initial π -NN-pair and final NN relative momenta and $\dot{\mathbf{S}}(S', S)$ denotes a rank one spin-transition operator connecting NN states with spin S and S' ; cf. Appendix 1 of I. The Cartesian vectors $\mathbf{V}(S', S)$ can be expressed in terms of the partial wave amplitudes A_i of Table I as follows:

$$\begin{aligned} \pi^+(\text{np})_{T=0} \rightarrow \text{pp}: \quad \mathbf{V}(1, 1) &= \sqrt{3}\eta A_1 \hat{\mathbf{q}}, \\ \mathbf{V}(0, 1) &= \sqrt{3}\eta(A_3 \boldsymbol{\kappa} + A_5 \mathbf{Q}) \end{aligned} \quad (2.2a)$$

$$\text{with } \mathbf{Q} = \frac{3}{\sqrt{2}} [\hat{\mathbf{q}}(\hat{\mathbf{q}} \cdot \boldsymbol{\kappa}) - \frac{1}{3} \boldsymbol{\kappa}],$$

$$\pi^+(\text{np})_{T=1} \rightarrow \text{pp}: \quad \mathbf{V}(1, 0) = \eta A_2 \hat{\mathbf{q}}, \quad (2.2b)$$

$$\begin{aligned} \pi^-(\text{pp}) \rightarrow \text{np}: \quad \mathbf{V}(1, 0) &= \frac{1}{\sqrt{2}} \eta (A_2 \hat{\mathbf{q}} - A_4 \boldsymbol{\kappa} - A_6 \mathbf{Q}). \\ & \quad (2.2c) \end{aligned}$$

η is an overall scale factor which we may choose at our convenience. The unpolarized differential cross section in the c.m. frame is given by

$$\frac{d\sigma}{d\Omega} [\pi^+(\text{np})_{T=0} \rightarrow \text{pp}] = \frac{2}{\kappa} [P_0 (|A_1|^2 + \kappa^2 (|A_3|^2 + |A_5|^2)) + P_2 \kappa^2 (|A_5|^2 + 2\sqrt{2} \text{Re} A_3 A_5^*)], \quad (2.6a)$$

$$\frac{d\sigma}{d\Omega} [\pi^+(\text{np})_{T=1} \rightarrow \text{pp}] = \frac{2}{\kappa} P_0 |A_2|^2, \quad (2.6b)$$

$$\begin{aligned} \frac{d\sigma}{d\Omega} [\pi^-(\text{pp}) \rightarrow \text{np}] &= \frac{1}{\kappa} [P_0 (|A_2|^2 + \kappa^2 (|A_4|^2 + |A_6|^2)) + 2\kappa P_1 \text{Re} A_2^* (A_4 + \sqrt{2} A_6) + P_2 \kappa^2 (|A_6|^2 + 2\sqrt{2} \text{Re} A_4 A_6^*)]. \\ & \quad (2.6c) \end{aligned}$$

Here, P_L stands for the L th Legendre polynomial in $\hat{\mathbf{k}} \cdot \hat{\mathbf{q}}$. In our approach, the A_i are treated as free parameters, to be inferred from experiment. Obviously, in reactions (2.6a) and (2.6c) the unpolarized differential cross section is not enough to pin down the A_i 's unambiguously: it

$$\sigma_{\text{abs}} = \frac{4\pi}{\kappa} \times \begin{cases} |A_1|^2 + \kappa^2 (|A_3|^2 + |A_5|^2) [\pi^+(\text{np})_{T=0} \rightarrow \text{pp}], \\ |A_2|^2 [\pi^+(\text{np})_{T=1} \rightarrow \text{pp}], \\ |A_2|^2 + \kappa^2 (|A_4|^2 + |A_6|^2) [\pi^-(\text{pp}) \rightarrow \text{np}]. \end{cases} \quad (2.7)$$

We have chosen the normalization of our amplitudes A_i with the purpose that they enter with equal weight here. Later on, we shall also need to know how the total absorption cross section for a 3S_1 pair depends on the M substate of the absorbing pair. Choosing the π -d relative momentum $\boldsymbol{\kappa}$ as quantization axis, we find

TABLE I. Allowed channels of the $\pi\text{NN} \rightarrow \text{NN}$ process, for pion s and p waves and NN pairs in initial s states.

i	l_π	$(\text{NN})_i$	$(\text{NN})_f$
1	0	3S_1	3P_1
2	0	1S_0	3P_0
3	1	3S_1	1S_0
4	1	1S_0	3S_1
5	1	3S_1	1D_2
6	1	1S_0	3D_1

$$\frac{d\sigma}{d\Omega} = f \frac{1}{2S+1} \sum_{S'} |\mathbf{V}(S', S)|^2, \quad (2.3)$$

with the kinematical factor

$$f = \frac{E(q)q}{8\pi^2 v_{\text{rel}}} \xrightarrow{\boldsymbol{\kappa} \rightarrow 0} \frac{M\mu\sqrt{\mu(4M+\mu)}}{16\pi^2 \kappa}. \quad (2.4)$$

μ and M are pion and nucleon masses, q is the final NN relative momentum as determined by energy conservation, and $E(q) = (M^2 + q^2)^{1/2}$. Following I, we adopt the normalization

$$\frac{1}{2} \kappa f \eta^2 = 1, \quad (2.5)$$

which yields the following expressions for the differential cross sections (2.3):

only gives two or three numbers (the Legendre coefficients α_L) as compared to five unknown (three complex amplitudes, minus an overall phase). The total absorption cross sections can be inferred from the P_0 coefficients in Eqs. (2.6):

$$\begin{aligned} \sigma_{M=0} &= \frac{4\pi}{\kappa} [|A_1|^2 + \kappa^2 (3|A_3|^2 + \frac{6}{5}|A_5|^2)], \\ \sigma_{M=\pm 1} &= \frac{4\pi}{\kappa} (|A_1|^2 + \frac{9}{10} \kappa^2 |A_5|^2). \end{aligned} \quad (2.8)$$

As expected, s absorption ($\sim A_1$) does not depend on

M . p absorption via A_5 yields a weak M dependence ($\sigma_0:\sigma_1=4:3$), whereas A_3 only contributes to the $M=0$ substate. The reason for this latter selection rule is the fact that since A_3 corresponds to a $^3S_1 \rightarrow ^1S_0$ transition and a pion p wave (cf. Table I), $\langle \mathbf{q} | t_{\text{abs}} | \boldsymbol{\kappa}, 1M \rangle$ can only be proportional to κ_{1M} ; for our choice of the z axis this vanishes unless $M=0$.

Via detailed balance, we can relate the total $\pi d \rightarrow \text{pp}$ cross section to the total $\text{pp} \rightarrow \pi d$ production cross section

$$\sigma_{\text{prod}} = \frac{3}{2}(\kappa^2/q^2)\sigma_{\text{abs}}. \quad (2.9)$$

Again, for later use, we have evaluated the total production cross sections for a deuteron in a definite M substate, using \mathbf{q} as the quantization axis (i.e., the relative pp momentum). The result is

$$\begin{aligned} \tilde{\sigma}_{M=0} &= g\kappa^2 |A_3 + \sqrt{2}A_5|^2, \\ \tilde{\sigma}_{M=\pm 1} &= \frac{1}{2}g(3|A_1|^2 + \kappa^2|\sqrt{2}A_3 - A_5|^2) \end{aligned} \quad (2.10)$$

with $g = 2\pi\kappa/q^2$.

Here, A_3 does not give rise to any M dependence since, after integrating over $d\Omega_{\mathbf{q}}$, there is no vector left. A_5 strongly favors $M=0$ production over $M=1$ (by a factor of 4), and A_1 , the s -wave production, is forbidden for $M=0$: It would require a $|10\rangle \rightarrow |10\rangle$ transition via a vector operator; cf. Eqs. (2.1) and (2.2a). Note that unlike the total cross sections (2.9), Eqs. (2.8) and (2.10) are no longer related by detailed balance because the M substates refer to different coordinate frames.

In I we estimated the s - and p -wave absorption strength parameters $|A_1|^2$ and $|A_3|^2 + |A_5|^2$ from the $\text{pp} \rightarrow \pi^+ d$ reaction near threshold, pionic He-atom data, and the imaginary part of the π -nucleus optical potential. For pions in flight, two questions arise immediately: What is the energy dependence of these parameters, and which extra information is contained in the differential cross sections?

For $\text{pp} \rightarrow \pi^+ d$, the usual threshold parametrization,

$$\sigma(\text{pp} \rightarrow \pi^+ d) = \alpha(\kappa/\mu) + \beta(\kappa/\mu)^3, \quad (2.11)$$

with $\alpha=0.18$ mb, $\beta=0.95$ mb (Ref. 11), falls short of the data at higher energies. Assuming that the energy dependence is entirely due to the p -wave parameter as suggested by the $\Delta N \rightarrow \text{NN}$ mechanism, we obtain the parameters listed in Table II (in paper I, different zero energy parameters have been assumed due to the use of the older values for α and β of Ref. 12).

For ^3He , Aniol *et al.*¹³ have extracted the quasi-free two-nucleon absorption cross section on np pairs of 10.2 (13.5) mb at 62.5 (82.8) MeV. Taking into account the number of 3S_1 pairs, 1.5, this translates into

$$|A_1|^2 + \kappa^2(|A_3|^2 + |A_5|^2) = \begin{cases} 0.036 \text{ fm} & \text{at 62.5 MeV,} \\ 0.056 \text{ fm} & \text{at 82.8 MeV.} \end{cases} \quad (2.12)$$

The value for $|A_1|^2$ is 0.015 fm at zero energy (cf. paper I). If we assume that this s -wave parameter does not increase with energy, we obtain the limits

TABLE II. Energy dependence of the p -wave strength $|A_3|^2 + |A_5|^2$ for the $\pi d \rightarrow \text{pp}$ process, calculated under the assumption that the s -wave strength remains at its zero energy value.

T_π (MeV)	$ A_3 ^2 + A_5 ^2$ (fm ⁶)
0	0.050
20	0.059
40	0.063
65	0.086
80	0.092

$$\begin{aligned} 0.048 \leq |A_3|^2 + |A_5|^2 \leq 0.081 \text{ fm}^3 & \text{ at 62.5 MeV,} \\ 0.067 \leq |A_3|^2 + |A_5|^2 \leq 0.091 \text{ fm}^3 & \text{ at 82.8 MeV.} \end{aligned} \quad (2.13)$$

The corresponding threshold value for ^3He is not known, but for ^4He it is 0.068 fm³. Thus, (2.13) suggests a weaker energy dependence than in the deuteron case.

As for the absorption parameters of the pion-nucleus optical potential, the MSU group¹⁴ has found that the values deduced from pionic atom data also give the correct order of magnitude of the total absorption cross sections, in the region 50–80 MeV. A quantitative conclusion cannot be drawn because the data¹⁵ have large uncertainties and tend to show larger π^+/π^- differences than the calculations.

The differential cross sections (usually parametrized via coefficients of Legendre polynomials α_L) contain additional information about the partial wave content of the absorption amplitudes. Both the $\pi^+ d \rightarrow \text{pp}$ and $\pi^+ ^3\text{He} \rightarrow 3p$ data are compatible with $\alpha_2/\alpha_0 \approx 1.1$, in the region between 60 and 80 MeV.^{13,16} The fact that the 1D_2 NN phase shifts have the largest inelasticities at low energies clearly shows the dominance of A_5 . If we then assume that the next important term in Eq. (2.6a) is the interference term linear in A_3 , we get the small ratio

$$\text{Re}(A_3/A_5) = \frac{\alpha_2/\alpha_0 - 1}{2\sqrt{2}} = 0.04. \quad (2.14)$$

The (π^- , np) coincidence measurements on ^3He provide complementary information on absorption from 1S_0 pairs.¹³ The total absorption cross section per pair is a factor 20 lower than for 3S_1 pairs, at 62.5 and 82.8 MeV, so that the amplitudes A_2 , A_4 , and A_6 are, on the average, suppressed by a factor 7.7 as compared to A_5 . The analysis of Ref. 13 suggests that none of these three amplitudes is as dominant as A_5 in the spin triplet case.

We now turn to a simple model which allows us to study gross features of pion absorption in complex nuclei in closed form. We consider a single pair of nucleons with quantum numbers $(n_1 l_1 n_2 l_2)_{LSJM}$ and T , bound in a harmonic oscillator well, and neglect all initial- and final-state interactions. This model has been analyzed for the case of stopped pions in I. After suitable changes in the kinematics, we can take over many of the results derived there. Let us denote by \mathbf{k} , \mathbf{p}_1 , and \mathbf{p}_2 the laboratory pion and nucleon momenta in the initial and final states, respectively, and introduce the “natural” QDM variables

$$\mathbf{P} = \mathbf{p}_1 + \mathbf{p}_2 - \mathbf{k}, \quad \mathbf{q} = \frac{1}{2}(\mathbf{p}_1 - \mathbf{p}_2), \quad \boldsymbol{\kappa} = \frac{2M\mathbf{k} - \omega\mathbf{P}}{2M + \omega}. \quad (2.15)$$

\mathbf{P} is the c.m. momentum of the NN pair prior to absorption (or minus the momentum of the recoiling nucleus), \mathbf{q} the relative momentum of the emitted nucleons, and $\boldsymbol{\kappa}$ the pion-NN-pair relative momentum, while $\omega = (\mu^2 + k^2)^{1/2}$. In these variables, the differential cross section for pion absorption on the bound pair is given by

$$\frac{d^3\sigma}{d\Omega_{\mathbf{P}} d\Omega_{\mathbf{q}} dP} = f \frac{P^2}{(2\pi)^3} I(\mathbf{P}, \mathbf{q}, \boldsymbol{\kappa}) \Big|_{q^2 = M(\omega - (\mathbf{P} + \mathbf{k})^2/4M)}, \quad (2.16)$$

with f from Eq. (2.4). $I(\mathbf{P}, \mathbf{q}, \boldsymbol{\kappa})$ stands for the appropriate spin sum over $|T_{fi}|^2$. There are four independent kinematical variables: the "recoil momentum" P and three angles needed to characterize the relative orientation of the vectors \mathbf{P} , \mathbf{q} , and $\boldsymbol{\kappa}$. Only two of these variables (P and $\cos\theta = \hat{\mathbf{P}} \cdot \hat{\mathbf{q}}$) survive in the limit of stopped pions.

In I we showed that $I(\mathbf{P}, \mathbf{q}, \boldsymbol{\kappa})$ factorizes into the probability of finding the NN pair with c.m. momentum P , times the spin sum of the elementary absorption process:

$$I(\mathbf{P}, \mathbf{q}, \boldsymbol{\kappa}) = \frac{|R_L^\beta(P)|^2}{4\pi} \frac{1}{|\Phi_{\text{rel}}(0)|^2} \tilde{I}(\hat{\mathbf{P}}, \mathbf{q}, \boldsymbol{\kappa}), \quad (2.17)$$

$$\tilde{I}(\hat{\mathbf{P}}, \mathbf{q}, \boldsymbol{\kappa}) = \text{Tr} \{ t_{\text{abs}}(\mathbf{q}, \boldsymbol{\kappa}) \rho_i^{\text{eff}}(\hat{\mathbf{P}}) t_{\text{abs}}^\dagger(\mathbf{q}, \boldsymbol{\kappa}) \}.$$

The functions $R_L^\beta(P)$ ($\beta = \{n_1 l_1 n_2 l_2\}$) in the harmonic oscillator model have been given in Appendix 2 of I, for the $0s$ and $0p$ shells. We have divided out the probability $|\Phi_{\text{rel}}(0)|^2$ of finding the two nucleons at zero separation, so that the $t_{\text{abs}}(\mathbf{q}, \boldsymbol{\kappa})$ of Eqs. (2.17) is consistent with the definition of t_{abs} in Eqs. (2.1) and (2.2). In cases where different n -quantum numbers can occur in $\Phi_{\text{rel}}(r)$, $|\Phi_{\text{rel}}(0)|^2$ stands for the appropriate average. Note the normalization condition

$$\int \frac{d^3P}{(2\pi)^3} \frac{|R_L^\beta(P)|^2}{4\pi} \frac{1}{|\Phi_{\text{rel}}(0)|^2} = 1. \quad (2.18)$$

$\rho_i^{\text{eff}}(\hat{\mathbf{P}})$ in (2.17) is the density matrix of the "deuteron" in the initial state. As discussed in I, it is 1 for 1S_0 pairs and for 3S_1 pairs with $L=0$, but contains a certain amount of tensor polarization for 3S_1 pairs with $L \neq 0$: In the standard notation,

$$\rho_i^{\text{eff}} = \frac{1}{3} \sum_{\lambda\mu} t_{\lambda\mu} \tau_{\lambda\mu}^\dagger, \quad (2.19)$$

$$t_{00} = 1, \quad t_{1\mu} = 0, \quad t_{2\mu} = \left[\frac{8\pi}{5} \right]^{1/2} \xi(L, J) Y_{2\mu}(\hat{\mathbf{P}}).$$

The factor $\xi(L, J)$ describes the state dependence of ρ_i^{eff} and can be written (for the $0s$ and $0p$ shells) as

$$\xi(L, J) = \frac{1}{2} \delta_{LJ} - (1 - \delta_{LJ}) \frac{3L - J + 1}{4(2J + 1)}. \quad (2.20)$$

Equations (2.17) reduce to the often assumed product form (recoil momentum distribution times unpolarized $\pi d \rightarrow \text{NN}$ differential cross section) in the cases $S=0$ or $L=0$. For spin triplet pairs and $L \neq 0$, however, the dif-

ferential cross section refers to a tensor-polarized "deuteron" and acquires a characteristic dependence on both the direction of \mathbf{P} and the state quantum numbers L, J . These polarization effects disappear if one integrates over $d\Omega_{\mathbf{P}}$.

The evaluation of $\tilde{I}(\hat{\mathbf{P}}, \mathbf{q}, \boldsymbol{\kappa})$, Eqs. (2.17), in terms of the vectors $\mathbf{V}(S', S)$ of Eqs. (2.2), is straightforward. For 1S_0 pairs, one gets trivially

$$\tilde{I}(\hat{\mathbf{P}}, \mathbf{q}, \boldsymbol{\kappa}) = |\mathbf{V}(1, 0)|^2, \quad (2.21)$$

with \mathbf{V} from Eqs. (2.2b) and (2.2c). This is proportional to the differential cross section of the elementary $\pi d \rightarrow \text{NN}$ process; cf. Eqs. (2.7b) and (2.7c). For 3S_1 pairs, the corresponding result is

$$\begin{aligned} \tilde{I}(\mathbf{P}, \mathbf{q}, \boldsymbol{\kappa}) = & \frac{1}{3} (|\mathbf{V}(0, 1)|^2 + |\mathbf{V}(1, 1)|^2) \\ & - \xi(L, J) \{ [|\hat{\mathbf{P}} \cdot \mathbf{V}(0, 1)|^2 - \frac{1}{3} |\mathbf{V}(0, 1)|^2] \\ & - \frac{1}{2} [|\hat{\mathbf{P}} \cdot \mathbf{V}(1, 1)|^2 \\ & - \frac{1}{3} |\mathbf{V}(1, 1)|^2] \}, \quad (2.22) \end{aligned}$$

with the \mathbf{V} 's from Eq. (2.2a). The first term on the right hand side of (2.22) yields again the unpolarized cross section, whereas the term multiplying $\xi(L, J)$ (which manifestly vanishes if one integrates over $d\Omega_{\mathbf{P}}$) arises from the polarization effects. Combining Eqs. (2.2), (2.16), (2.21), and (2.22), we have arrived at the solution of our model problem. Already in this idealized case, we notice a more subtle interplay between the elementary absorption process and the angular momentum structure of the transition considered than has been commonly assumed. Two qualitative new features are predicted for absorption on 3S_1 pairs with $L \neq 0$: a characteristic state dependence [via $\xi(L, J)$] very different from the trivial dependence through $|R_L^\beta(P)|^2$, and a dependence on the direction of \mathbf{P} , or, equivalently, the recoil momentum. We illustrate the size of these effects by evaluating (2.22) for the important special case of a pure A_5 absorption amplitude:

$$\begin{aligned} \tilde{I}(\hat{\mathbf{P}}, \mathbf{q}, \boldsymbol{\kappa}) = & \frac{1}{2} \eta^2 \kappa^2 |A_5|^2 \\ & \times \{ [1 + \xi(L, J)] [1 + 3(\hat{\mathbf{q}} \cdot \hat{\boldsymbol{\kappa}})^2] \\ & - 3\xi(L, J) (3\hat{\mathbf{q}} \cdot \hat{\mathbf{P}} \hat{\mathbf{q}} \cdot \hat{\boldsymbol{\kappa}} - \hat{\mathbf{P}} \cdot \hat{\boldsymbol{\kappa}}) \}. \quad (2.23) \end{aligned}$$

Considering that $\xi(L, J)$ of Eq. (2.19) ranges from $-\frac{1}{2}$ to $+1$ for s - and p -shell nucleons, it is clear that the dependence on $\hat{\mathbf{P}}$ and L, J can be very strong.

Instructive expressions can be derived by integrating the cross section (2.16) over some of the kinematical variables. Specifically, we focus on 3S_1 pairs and evaluate the distributions in all three angles which occur naturally in the QDM: $\hat{\mathbf{q}} \cdot \hat{\boldsymbol{\kappa}}$, $\hat{\mathbf{P}} \cdot \hat{\boldsymbol{\kappa}}$, and $\hat{\mathbf{q}} \cdot \hat{\mathbf{P}}$.

A. $\hat{\mathbf{q}} \cdot \hat{\boldsymbol{\kappa}}$ distribution

This angle is the one relevant for the elementary $\pi d \rightarrow \text{NN}$ cross section in the c.m. system. Upon integrating (2.16) over $dP d\Omega_{\mathbf{P}}$, neglecting the P dependence contained in κ and q , we simply get

$$\frac{d\sigma}{d\hat{\mathbf{q}}\cdot\hat{\mathbf{k}}} = \frac{d\sigma}{d\cos\theta_{\text{c.m.}}} \Big|_{\pi d \rightarrow \text{NN}} \quad (2.24)$$

The distribution (2.24) is independent of the particular transition and directly reflects the underlying absorption process.

B. $\hat{\mathbf{P}}\cdot\hat{\mathbf{k}}$ distribution

The distribution in $\hat{\mathbf{P}}\cdot\hat{\mathbf{k}}$ is closely related to the recoil angle distribution ($\cos\theta_R = \hat{\mathbf{P}}_R\cdot\hat{\mathbf{k}}$), since

$$\hat{\mathbf{P}}_R\cdot\hat{\mathbf{k}} = -\hat{\mathbf{P}}\cdot\hat{\mathbf{k}} + O(\omega/M). \quad (2.25)$$

The angular average over $\tilde{I}(\hat{\mathbf{P}}, \mathbf{q}, \kappa)$ needed here is

$$\begin{aligned} \frac{1}{4\pi\eta^2} \int d\Omega_{\mathbf{q}} \tilde{I}(\hat{\mathbf{P}}, \mathbf{q}, \kappa) &= |A_1|^2 + \kappa^2 (|A_3|^2 + |A_5|^2) \\ &\quad - \xi(L, J) \kappa^2 \left(\frac{1}{5} |A_5|^2 + 2 |A_3|^2 \right) \\ &\quad \times P_2(\hat{\mathbf{P}}\cdot\hat{\mathbf{k}}). \end{aligned} \quad (2.26)$$

Including the kinematical factors of Eq. (2.16) and using (2.8) for the total absorption cross section on a deuteron in a definite M substate, σ_M , we can eliminate the amplitudes A and find the compact expression

$$\frac{d\sigma}{d\hat{\mathbf{P}}\cdot\hat{\mathbf{k}}} = \frac{1}{6} [\sigma_0 + 2\sigma_1 - 2\xi(L, J)(\sigma_0 - \sigma_1)P_2(\hat{\mathbf{P}}\cdot\hat{\mathbf{k}})]. \quad (2.27)$$

The predicted $\hat{\mathbf{P}}\cdot\hat{\mathbf{k}}$ dependence turns out to be rather weak for A_5 dominance:

$$\frac{d\sigma}{d\hat{\mathbf{P}}\cdot\hat{\mathbf{k}}} = 2\pi\kappa |A_5|^2 \left[1 - \frac{1}{5} \xi(L, J) P_2(\hat{\mathbf{P}}\cdot\hat{\mathbf{k}}) \right]. \quad (2.28)$$

C. $\hat{\mathbf{P}}\cdot\hat{\mathbf{q}}$ distribution

Following the convention for stopped pions, we shall refer to the angle between $\hat{\mathbf{P}}$ and $\hat{\mathbf{q}}$ as θ . We can obtain the θ distribution for pions in flight by integrating over $d\Omega_{\kappa}$. The angular average yields

$$\begin{aligned} \frac{1}{4\pi\eta^2} \int d\Omega_{\kappa} \tilde{I}(\hat{\mathbf{P}}, \mathbf{q}, \kappa) &= |A_1|^2 + \kappa^2 (|A_3|^2 + |A_5|^2) \\ &\quad + \xi(L, J) \{ |A_1|^2 - \kappa^2 [|A_5|^2 + 2\sqrt{2} \text{Re}(A_3 A_5^*)] \} \\ &\quad \times P_2(\hat{\mathbf{P}}\cdot\hat{\mathbf{q}}), \end{aligned} \quad (2.29)$$

where we have again neglected $O(\omega/M)$ corrections. Comparing (2.29) with the expressions (2.10) for the production cross sections of polarized deuterons ($\bar{\sigma}_M$) in the inverse reaction $pp \rightarrow \pi^+ d$, we get an expression closely analogous to (2.27):

$$\frac{d\sigma}{d\cos\theta} = \frac{1}{3} \frac{q^2}{\kappa^2} [\bar{\sigma}_0 + 2\bar{\sigma}_1 - 2\xi(L, J)(\bar{\sigma}_0 - \bar{\sigma}_1)P_2(\cos\theta)]. \quad (2.30)$$

By specializing to the cases of pure A_1 or A_5 amplitudes, one can recover here the θ distributions for s and p absorption of stopped pions given explicitly in Table 2 of I.

III. COMPARISON WITH THE $^{16}\text{O}(\pi^+, pp)^{14}\text{N}$ DATA AT 59.6 MeV: QUALITATIVE FEATURES

Recently, the first high resolution coincidence data for absorption of pions in flight have become available from LAMPF. Wharton *et al.*⁸ have studied the reaction $^{16}\text{O}(\pi^+, pp)^{14}\text{N}$ at 59.6 MeV and have presented detailed results for two specific final states of ^{14}N , the ground state and the 3.9 MeV excited state (both 1^+ , $T=0$). A comparison between these two transitions is appealing because they are predicted to involve almost pure $L=2$ (g.s.) [$L=0$ (3.9 MeV state)] transfer.¹⁷ The transition to the 3.9 MeV state had already been measured before with stopped pions.⁵ In I we showed that these zero energy data can be well understood with the QDM. In this section we shall confront the QDM in the simplified form of Sec. II with the new 60 MeV data from LAMPF, concentrating on the qualitative aspects. Such a comparison is greatly facilitated by the fact that Wharton *et al.* have parametrized their data in a simple way, guided by the QDM. A more quantitative study of certain aspects and all actual cross section calculations will be deferred to Sec. IV, where we shall employ a distorted wave approach. For the moment, we tacitly assume that we may identify the asymptotic pion and nucleon momenta with the variables entering the elementary absorption process, and do not worry about absolute normalizations.

The data of Ref. 8 have been parametrized in terms of a "T matrix" of the following form:

$$|T|^2 = f(P_R) [1 + a_2 P_2(\hat{\mathbf{k}}\cdot\hat{\mathbf{q}})] g(\mathbf{P}_R, \hat{\mathbf{p}}_1, \hat{\mathbf{p}}_2) \quad (\mathbf{P}_R = -\mathbf{P}), \quad (3.1a)$$

with

$$\begin{aligned} g(\mathbf{P}_R, \hat{\mathbf{p}}_1, \hat{\mathbf{p}}_2) &= N(P_R) [1 + B(P_R) \hat{\mathbf{P}}_R \cdot \hat{\mathbf{p}}_1 \hat{\mathbf{P}}_R \cdot \hat{\mathbf{p}}_2] \\ &\quad \times [1 + C(P_R) \cos\theta_R], \\ N(P_R) &= [1 - B(P_R)/3]^{-1}, \quad \cos\theta_R = \hat{\mathbf{P}}_R \cdot \hat{\mathbf{k}}. \end{aligned} \quad (3.1b)$$

Since the phase space factor has been pulled out already, we can directly compare $|T|^2$ of (3.1a) with the spin sum $I(\mathbf{P}, \mathbf{q}, \kappa)$ introduced in Eq. (2.16). The various functions and coefficients appearing in Eqs. (3.1) will be discussed as we go along. We proceed in two steps: First, we compare the integral of $|T|^2$ over the recoil angles with the corresponding QDM prediction. In this way we eliminate the complicated function g in (3.1b) and the tensor polarization effects discussed in Sec. II. In the second step we shall examine in detail the recoil angle dependence of $|T|^2$ and $I(\mathbf{P}, \mathbf{q}, \kappa)$.

Upon integrating $|T|^2$ of (3.1a) over $d\Omega_{\mathbf{p}}$, we obtain an expression of the same general structure as in the QDM of Sec. II; cf. Eqs. (2.17) and (2.22):

$$\int |T|^2 d\Omega_{\mathbf{p}} \sim f(P_R) [1 + a_2 P_2(\hat{\mathbf{k}}\cdot\hat{\mathbf{q}})], \quad (3.2a)$$

$$\int I(\mathbf{P}, \mathbf{q}, \kappa) d\Omega_{\mathbf{p}} \sim |R_L^\beta(P)|^2 [\alpha_0 + \alpha_2 P_2(\hat{\mathbf{k}}\cdot\hat{\mathbf{q}})]. \quad (3.2b)$$

Equation (3.2a) follows from (3.1a) because

$$\int d\Omega_{pg}(\mathbf{P}_R, \hat{\mathbf{p}}_1, \hat{\mathbf{p}}_2) = \text{const} \quad (3.3)$$

by construction. The Legendre coefficients α_L entering (3.2b) can be read off Eq. (2.6a). Obviously, $f(P_R)$ corresponds to the deuteron momentum distribution, whereas the $\hat{\mathbf{k}} \cdot \hat{\mathbf{q}}$ dependence reflects the unpolarized elementary $\pi d \rightarrow pp$ cross section. The best fit parameters for a_2 are (within the uncertainties) consistent with the value 1.1 of the free $\pi d \rightarrow pp$ reaction, confirming the dominance of the amplitude A_5 also inside the nucleus. As far as $f(P_R)$ is concerned, we note that both $L=0$ and 2 transfer can contribute for 1^+ states. If we rely on the 2-cfp's of Cohen and Kurath¹⁷ (CK), we obtain the recoil momentum distributions shown in Figs. 1 and 2, together with the data (arbitrary normalization). The agreement in shape is reasonable for the 3.9 MeV state, but there is a rather dramatic discrepancy for the g.s. at small P_R . Within the QDM there are, in principle, two ways of generating a peak at $P_R=0$: either one increases the $L=0$ component in the wave function as compared to the CK results, or one assumes that absorption on pairs different from 3S_1 pairs is important.

The first alternative seems to be in conflict with other two-particle transfer reactions.¹⁸ In order to illustrate the

amount of $L=0$ component needed, we have nevertheless varied the $(L=0)/(L=2)$ transfer ratio to get the qualitative fit of Fig. 3 (solid curve). We have to increase the ratio $c_0/c_2 = -0.078$ (CK) of the 2-cfp's by a factor of 2.7. The second possible explanation has been advocated in Ref. 8. $L=2$ transfer implies a 3S_1 pair with an $L=2$ c.m. wave function, or a 3D_1 pair with $L=0$. The latter component is equally strong in the nuclear wave function, but not expected to show up, because absorption on a d pair should be dynamically suppressed. If we allow the ratio of absorption cross sections to vary freely, we can arrive at the shape of $f(P_R)$ shown as the dashed curve in Fig. 3 (the difference in shape between the two curves is due to different n -quantum numbers involved). We need

$$\frac{d\sigma/d\Omega[^3D_1]}{d\sigma/d\Omega[^3S_1]} \approx 0.35 \quad (3.4)$$

on the average, in the angular region covered by the experiment ($\theta_{c.m.} = 63^\circ, \dots, 90^\circ$). The angular dependence of the two cross sections would be the same if both were dominated by the $^5S_2(\Delta N) \rightarrow ^1D_2(NN)$ transition [this would also be consistent with the finding that a_2 in Eq. (3.1a) is approximately the same in both transitions]. Then the ratio (3.4) would directly reflect the ratio of total absorption cross sections, and be at least 3 times larger than expected (see, for instance, Fig. 5 of Ref. 19).

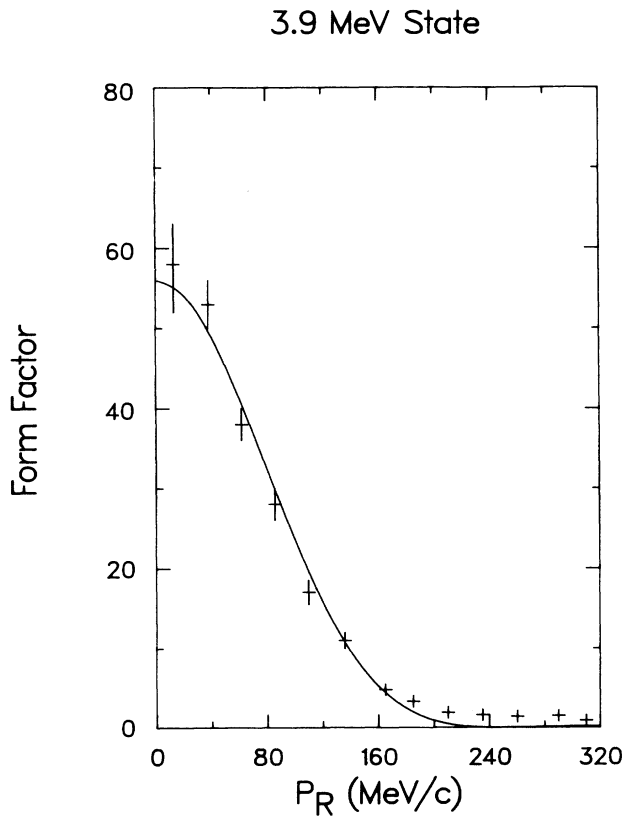


FIG. 1. Form factor (recoil momentum distribution) for the 3.9 MeV state, calculated from the CK wave functions, as compared to the data of Ref. 8, in the units employed there. Normalization fitted to the data.

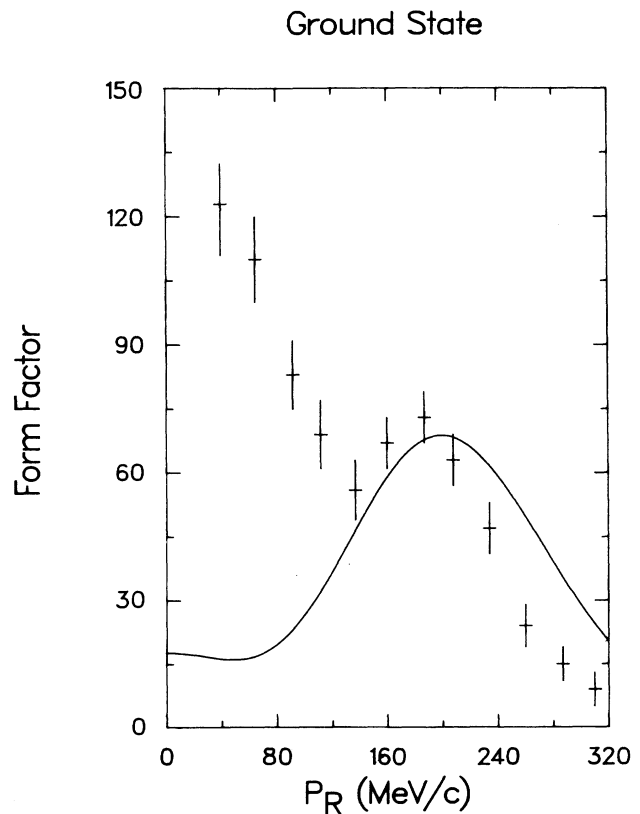


FIG. 2. Same as Fig. 1, but transition to the ground state shown.

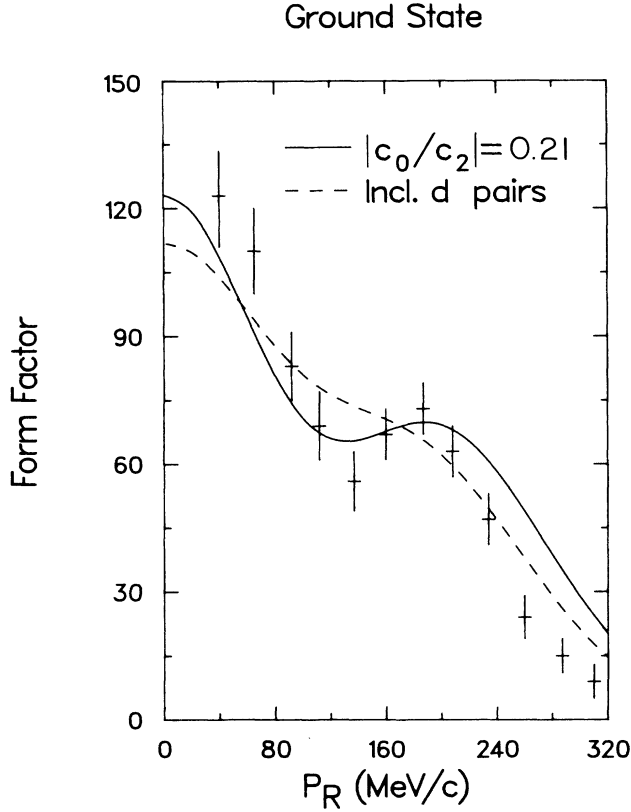


FIG. 3. Same as Fig. 2, but peak at $P_R=0$ fitted by adding an extra $L=0$ component in the wave function (cfp ratio $c_0/c_2=-0.21$), or including absorption on pairs in relative d states.

We now turn to the extra dependence of $|T|^2$ on the kinematical variables contained in $g(\mathbf{P}_R, \hat{\mathbf{p}}_1, \hat{\mathbf{p}}_2)$, Eq. (3.1b). g has been introduced by the authors of Ref. 8 to account for unexpected strong state- and recoil-angle dependence of the data. The term proportional to $C(P_R)$ can be understood as a consequence of the energy dependence of the elementary $\pi d \rightarrow pp$ cross section. Since this energy dependence enters only via the transformation from the lab to πd c.m. system, the effect on the θ_R dependence is rather weak. In Sec. II we ignored such nonstatic corrections for the sake of simplicity, but we shall include them in the more detailed calculations of Sec. IV.

The most intriguing term in g is the one proportional to $B(P_R)$, where $B(P_R)$ depends strongly on P_R and the transition considered (see Fig. 6 of Ref. 8). Before comparing this term to the QDM, it is necessary to eliminate the lab momenta $\mathbf{p}_1, \mathbf{p}_2$ in favor of natural QDM variables. Notice that

$$\hat{\mathbf{p}}_1 \cdot \hat{\mathbf{P}}_R \hat{\mathbf{p}}_2 \cdot \hat{\mathbf{P}}_R = -(\hat{\mathbf{q}} \cdot \hat{\mathbf{P}}_R)^2 + \mathcal{O} \left(\left[\frac{\mathbf{k} - \mathbf{P}_R}{2q} \right]^2 \right). \quad (3.5)$$

A crude but useful approximation is to keep only the leading term on the right hand side. For the 3.9 MeV state,

$B(P_R) \approx -1.4$ between $P_R=130$ and 180 MeV/ c , and is small outside of this interval. Hence, g yields the dependence

$$g \sim 1 + 1.4(\hat{\mathbf{q}} \cdot \hat{\mathbf{P}}_R)^2 \quad [3.9 \text{ MeV state, } 130 \leq P_R \leq 180 \text{ MeV}/c]. \quad (3.6)$$

Taking into account the fact that the experimental setup favors in-plane geometry and angles $\theta_{c.m.}$ in the vicinity of 90° , this yields the θ_R dependence

$$g \sim 1 + 1.4 \sin^2 \theta_R \sim 1 - 0.6 \cos^2 \theta_R, \quad (3.7)$$

in qualitative agreement with Fig. 8 of Ref. 8. By contrast, the QDM predicts no θ_R dependence at all for a pure $L=0$ transition. We shall comment on the role of possible small $L=2$ admixtures below.

For the ground state, $B(P_R)$ is 0 below 170 MeV/ c , then rises rather suddenly to ~ 1 , where it stays above 200 MeV/ c . Therefore,

$$g \sim 1 - (\hat{\mathbf{q}} \cdot \hat{\mathbf{P}}_R)^2 \sim \cos^2 \theta_R \quad [\text{g.s., } P_R \geq 200 \text{ MeV}/c], \quad (3.8)$$

where we have again specialized to the in-plane geometry and $\theta_{c.m.}=90^\circ$. This distribution agrees roughly with Fig. 7 of Ref. 8. Let us assume that the high recoil momentum data are predominantly $L=2$ transfer. The QDM of Sec. II predicts, for $L=2, J=1$, and a pure A_5 amplitude [cf. Eq. (2.23)],

$$\begin{aligned} I(\mathbf{P}, \mathbf{q}, \boldsymbol{\kappa}) &\sim 1 + 3(\hat{\mathbf{q}} \cdot \hat{\boldsymbol{\kappa}})^2 + 3(3\hat{\mathbf{q}} \cdot \hat{\mathbf{P}} \hat{\boldsymbol{\kappa}} \cdot \hat{\mathbf{P}} - \hat{\mathbf{P}} \cdot \hat{\boldsymbol{\kappa}})^2 \\ &\sim 1 + 3 \cos^2 \theta_R \quad (\theta_{c.m.}=90^\circ). \end{aligned} \quad (3.9)$$

Near $\theta_{c.m.}=90^\circ$, this is remarkably similar to (3.8), a first hint that the predicted polarization effects may indeed be visible in the data. Inspection of Eq. (3.9) shows that if our interpretation is correct, the strong θ_R dependence observed is a special feature of kinematics around $\theta_{c.m.}=90^\circ$. Indeed, if one would integrate (3.9) over all c.m. angles, the θ_R dependence would be almost completely washed out [see Eq. (2.28)]. The parametrization of Wharton *et al.*, on the other hand, suggests a strong θ_R dependence at all c.m. angles,

$$|T|^2 \sim [1 + 3(\hat{\mathbf{q}} \cdot \hat{\boldsymbol{\kappa}})^2][1 - (\hat{\mathbf{P}}_R \cdot \hat{\mathbf{q}})^2]. \quad (3.10)$$

In the QDM this could only happen in the unlikely case that $A_3 \gg A_5$. However, we should bear in mind that the parametrization (3.10) is only backed up by experimental data in a rather small interval of c.m. angles.

A disturbing feature of this comparison is the fact that the 3.9 MeV state also displays a conspicuous θ_R dependence, contrary to the expectations for $L=0$ transitions. This raises the question whether small $L=2$ admixtures (present for instance in the CK wave functions) could be responsible for such an effect. In order to answer this question, we have generalized the schematic model of Sec. II for 1^+ states, allowing arbitrary admixtures of $L=0$ and 2 pairs. As is shown in the Appendix, the effective density matrix ρ_i^{eff} of the deuteron in the initial state can be evaluated along similar lines as before. The main

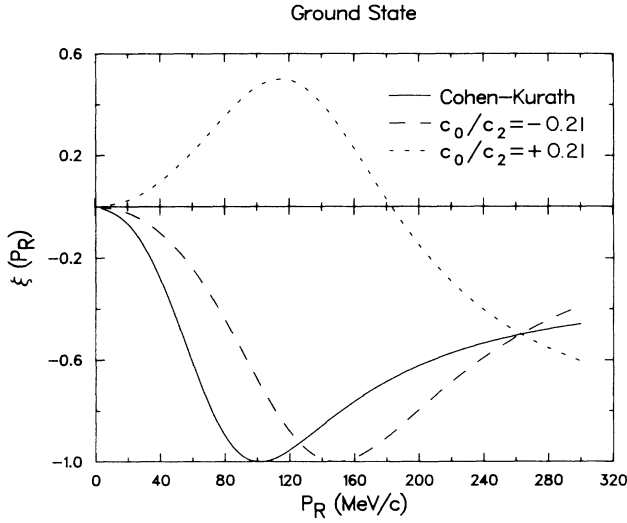


FIG. 4. $\xi(P_R)$ calculation for CK wave functions (solid curve), and for a ratio of cfp's of $c_0/c_2 = -0.21$ (long dashes) or $c_0/c_2 = +0.21$ (short dashes).

modification is the fact that the parameter $\xi(L, J)$ of Eq. (2.20) now becomes P_R dependent. We find

$$\xi(P_R) = -\frac{1}{2} \left[\frac{(c_2 R_2)^2 - \sqrt{8} c_0 R_0 c_2 R_2}{(c_2 R_2)^2 + (c_0 R_0)^2} \right] (1^+ \text{ state}). \quad (3.11)$$

Here, $R_L \equiv R_L^{(0101)}(P_R)$ is the wave function of Appendix 2 of I, and c_L denotes the 2-cfp in LS coupling. If we evaluate $\xi(P_R)$ for the 3.9 MeV state using CK wave functions ($c_0 = 0.2013$, $c_2 = 0.0352$), we find

$$\xi(P_R) = \begin{cases} 0.028 & \text{at } 100 \text{ MeV}/c, \\ 0.080 & \text{at } 150 \text{ MeV}/c, \\ 0.226 & \text{at } 200 \text{ MeV}/c. \end{cases} \quad (3.12)$$

The experimental θ_R distribution (3.7) corresponds to $\xi \approx 0.25$. Hence, the sign of the effect (which is determined by the relative sign between c_0 and c_2 , since the interference term dominates) is correct, but the magnitude too small.

As a second illustration of Eq. (3.11), we show in Fig. 4 the function $\xi(P_R)$ for the ground state transition, using either the CK wave functions or the wave function with the strong $L=0$ admixture used in Fig. 3. We first notice that, for $P_R > 200$ MeV/c, all three curves agree roughly with the value $\xi = -\frac{1}{2}$ for a pure $L=2$ transition, so that the prediction (3.9) is very stable in this region. Below 200 MeV one would also expect strong θ_R dependence from Fig. 4, whereas the data require $B(P_R) \approx 0$, i.e., isotropy. This may be taken as an indication that the large cross section observed at small P_R cannot be interpreted in terms of $L=0$ admixtures to the wave function.

IV. DISTORTED WAVE CALCULATIONS

Once the elementary absorption operator has been chosen, the distortion effects of the pion in the initial state and the two protons in the final state can be taken into account numerically, using well established techniques. The calculational method and approximations used here are similar to those described in I, so thus we need to discuss only the modifications. The partial wave amplitudes a_i [which differ from the A_i by not containing the bound state wave function; cf. Eq. (2.4) of I] are assumed to have the simple functional form

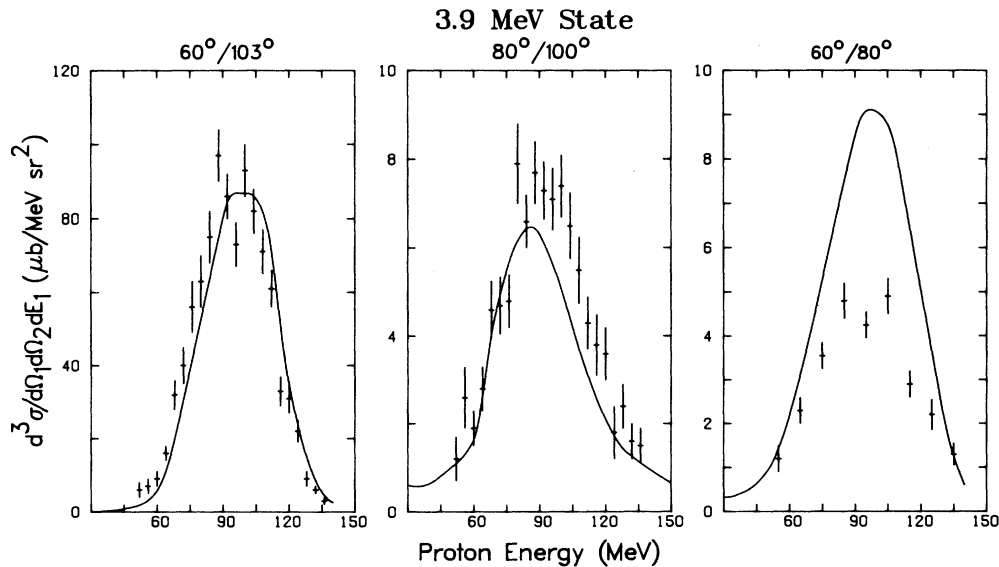


FIG. 5. Results of the standard calculation for the transition to the 3.9 MeV state, compared to the data of Ref. 8 at three pairs of angles (θ_1, θ_2) for the emitted protons.

$$\alpha_i(q', q, \eta) = \bar{\alpha}_i \exp(-\beta^2 q^2), \quad (4.1)$$

with the range parameter $\beta=1$ fm. This yields a ratio of 1.1 for the absorption cross section on $n=0$ and 1 3S_1 pairs in ^{16}O , as compared to $\frac{2}{3}$ in the zero-range limit. Furthermore, only the dominant $i=5$ absorption channel ($^3S_1 \rightarrow ^1D_2$) has been kept tentatively. When evaluating the DWIA matrix elements, the nucleon momenta in the transition operator (2.1) and (2.2) are replaced by the asymptotic momenta, whereas the pion momentum is treated rigorously as a gradient acting on the distorted wave. This partial factorization can be justified if the \mathbf{k} factors from p -wave absorption are indeed the most rapidly varying functions, at low energies. Besides, it is also required for consistency with the pion optical potential used here. This latter is the MSU potential of Stricker, McManus, and Carr.¹⁴ Proton final state interactions are described via the Engelbrecht-Fiedeldej potential,²⁰ including the Coulomb interaction. The nuclear structure input is taken from Cohen and Kurath¹⁷ unless indicated otherwise; harmonic oscillator bound-state wave functions with $b=1.72$ fm and the usual c.m. correction have been employed. We will refer to a calculation, to which the physical input is as indicated in this paragraph, as a "standard" calculation. All calculations are carried out in coordinate space after a standard partial wave decomposition (for more details, see Ref. 21).

We now turn to the results of the calculations. Let us first consider the transition to the 3.9 MeV 1^+ state in ^{14}N . Figure 5 shows the data of Wharton *et al.*⁸ at three pairs of detector angles, in comparison with DWIA calculations normalized to the peak height of the $60^\circ/103^\circ$ data (a point of practically zero recoil momentum). We disregard the fourth set of angles ($100^\circ/100^\circ$), where the kinematics is too far away from the quasi-free point ($P_R \geq 300$ MeV/c). The data are consistent with the assumed $L=0$ dominance, confirming similar findings with

stopped pions (I). The value of $|\bar{\alpha}_5|^2$ needed to reproduce the absolute normalization is

$$|\bar{\alpha}_5|^2 = 15.6 \text{ fm}^6. \quad (4.2)$$

For comparison, the limits deduced from the 62.5 MeV ^3He data, Eq. (2.13), correspond to values of $|\bar{\alpha}_5|^2$ between 7.9 and 13.3 fm. Since we have neglected s -wave absorption altogether here, we should compare the value (4.2) with 13.3 fm for ^3He , indicating very good consistency between these different data. However, one must be aware that in detail this comparison depends on the assumed value of 1 fm for the range parameter β .

To illustrate the importance of distortion effects, we note that the peak value in Fig. 5(a) is decreased by a factor of 1.9 as compared to a PWIA (partial wave impulse approximation) calculation (15–20% increase due to pion distortion, a factor of 2.3 decrease due to nucleon distortion).

Furthermore, the relative height of the peaks at different detector settings is rather sensitive to the assumed range parameter β of Eq. (4.1). Thus for instance, the peak cross section at $80^\circ/100^\circ$ ($60^\circ/80^\circ$) would decrease by 40% (30%) relative to the peak at $60^\circ/103^\circ$ in the zero range limit.

In Fig. 6 we compare the $\theta_{c.m.}$ dependence of the data for the 3.9 MeV state with the DWIA prediction, using again a pure A_5 amplitude. $\theta_{c.m.}$ characterizes the elementary $\pi d \rightarrow pp$ reaction in the c.m. system. The data are presented in the form of the smooth "TRIDIF" parametrization of Ref. 8. The excellent agreement in shape shows no indication for the presence of other significant amplitudes. Hence, from now on we shall keep A_5 fixed to the value obtained from Fig. 5(a), and set $A_1 = A_3 = 0$.

As the last result for the 3.9 MeV state, Fig. 7 displays the dependence on the recoil angle θ_R for two values of P_R and two values of $\theta_{c.m.}$. The TRIDIF interpolation of

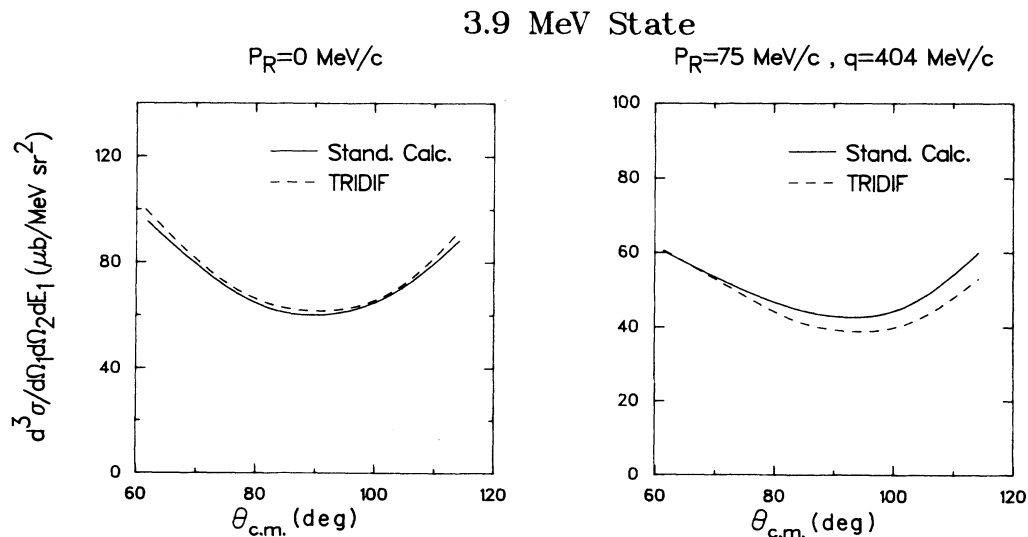


FIG. 6. $\theta_{c.m.}$ dependence of the standard calculation for the 3.9 MeV state, calculated at $P_R=0$ and at 75 MeV/c, $q=404$ MeV/c (solid curves), compared to the data of Ref. 8, here represented by the TRIDIF parametrization (dashed curves).

the data is shown together with PWIA and DWIA calculations [both normalized in the same way to Fig. 5(a)]. The PWIA predicts a much weaker θ_R dependence than actually observed, in accordance with the dominant $L=0$ character of the transition (see Sec. III). However, distortion effects induce a variation of the correct shape, reducing the discrepancies between the PWIA and experiment. The sensitivity to distortion effects is unusually strong here, presumably because we are in a kinematical region away from the quasi-free kinematics, where the recoil momentum distribution is rapidly varying. Apparently, it is dangerous to simply identify the asymptotic momenta with the variables governing the QDM inside the nucleus: this may give rise to a spurious dependence on certain variables like θ_R .

The results shown in Figs. 5–7 demonstrate that the data for the 3.9 MeV 1^+ state are consistent with the QDM, provided one takes into account finite range and distortion effects. The absorption strength parameter that we need, when we set the range parameter $\beta=1$ fm, is slightly larger than the one suggested by the ^3He data at 62 MeV.

Figure 8 is the analogue of Fig. 5, but for the transition to the g.s. of ^{14}N . According to our discussion in Sec. III, the CK wave functions do not reproduce the observed recoil momentum distribution, so we have very little resemblance between theory and experiment, both in shape and magnitude (the normalization is still determined by the 3.9 MeV state). To check whether the problem can be solved by modifying the nuclear structure in-

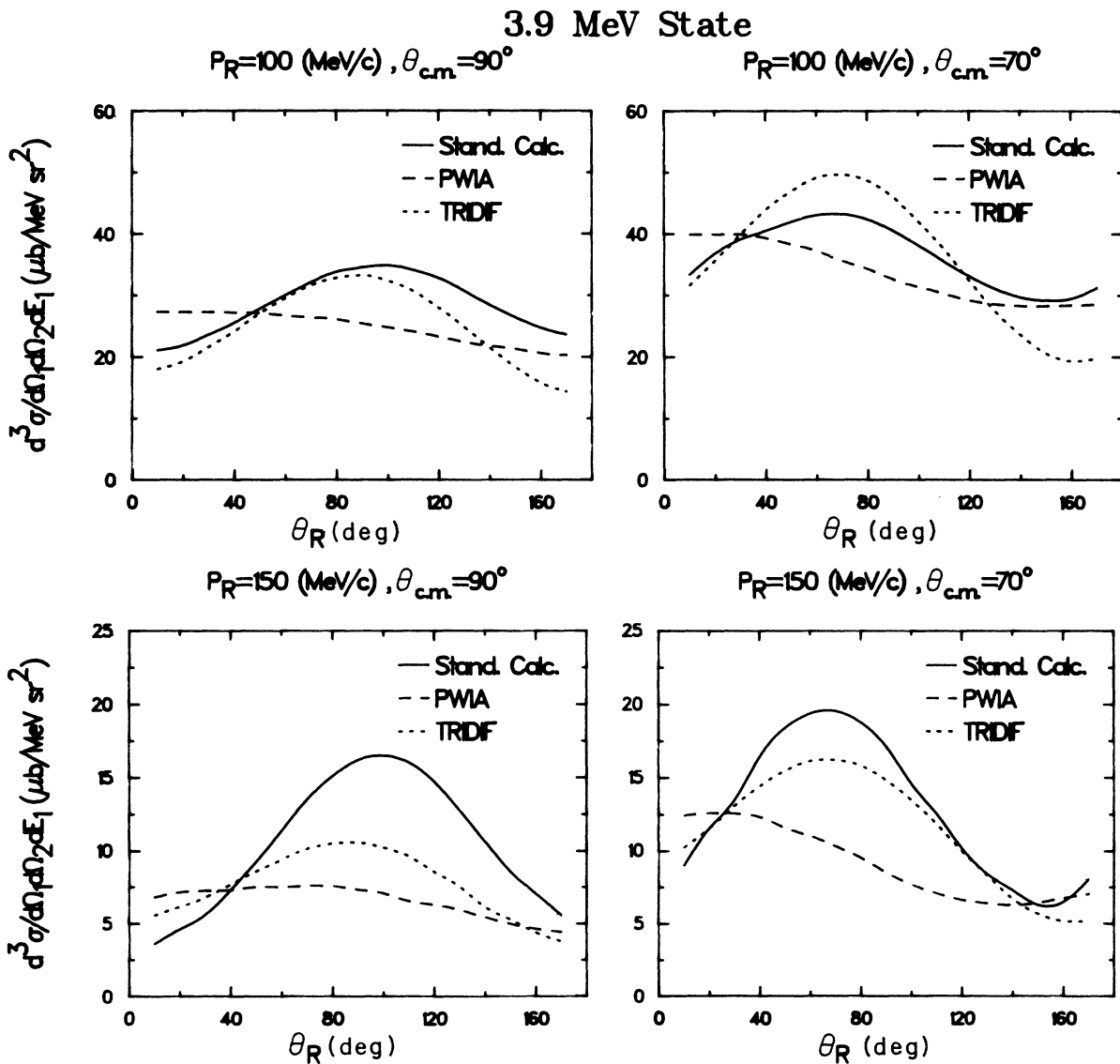


FIG. 7. θ_R dependence of the transition to the 3.9 MeV state. Solid curves give the results of the standard calculation. Also shown are the results of a PWIA calculation (long dashes) and the data, as represented by the TRIDF parametrization (short dashes). Panels (a)–(d) present results at four pairs of values for P_R and $\theta_{\text{c.m.}}$.

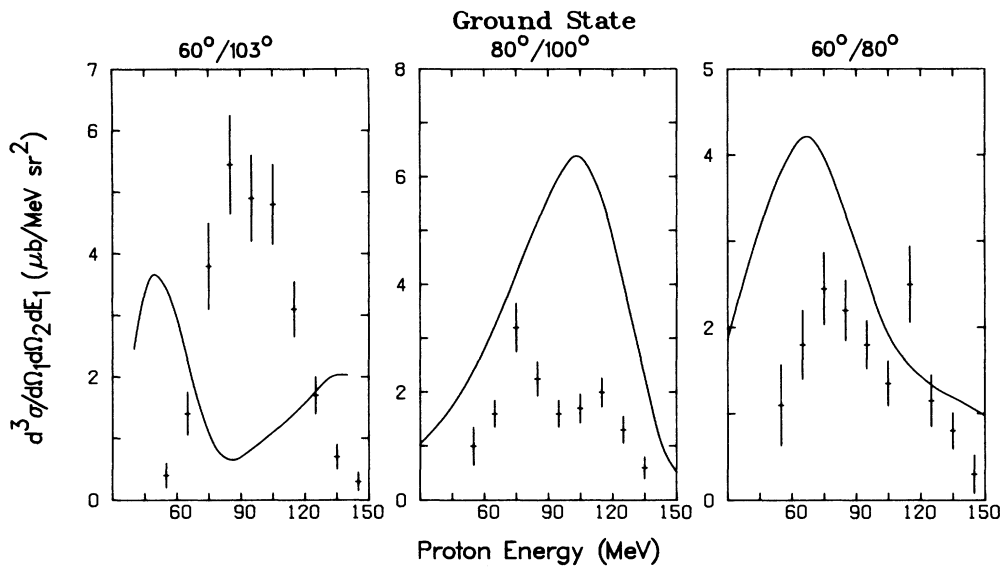


FIG. 8. Same as Fig. 5, but results for the transition to the ground state shown.

put only, we have also performed calculations with a strong $L=0$ admixture, similar to that used in Fig. 3. Figure 9 shows our results for both destructive and constructive interference between $L=0$ and 2 components. This is evidently not sufficient to resolve the discrepancies. The challenge of the $60^\circ/103^\circ$ cross section for instance, is not only to produce a peak at $P_R=0$, but also to eliminate the double-hump structure resulting from the $L=2$ component of the recoil wave function. In the TRIDIF parametrization of the data, this is achieved by invoking strong simultaneous dependence on P_R and θ_R . In the QDM, this would require strong interference effects between different reaction contributions.

In Fig. 10 we show the θ_R dependence at $P_R=225$ MeV/c, for two c.m. angles. In striking contrast to the poor cross-section results, the DWIA predicts very well the qualitative behavior of the θ_R distribution, confirming the discussion of the preceding section. Apparently, the polarization effects present in the QDM for transitions with $L=2$ are clearly visible, provided one focuses on events with large recoil momenta. It is worth noting that distortion has rather little effect on the shape of the θ_R distributions here, unlike in the case of the 3.9 MeV state. This is presumably due to the fact that we are close to the maximum of the $L=2$ recoil momentum distribution, as compared to the tail of the $L=0$ distribution in the previ-

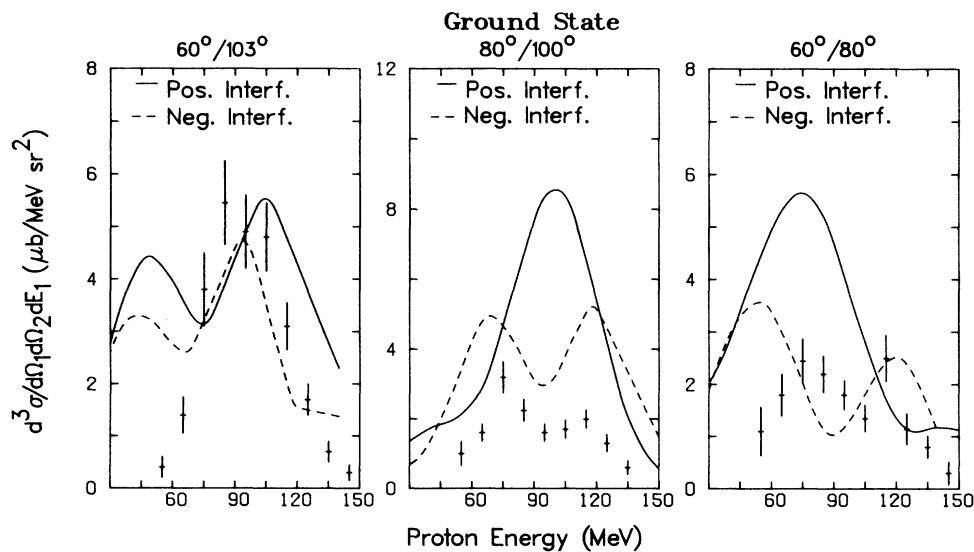


FIG. 9. Same as Fig. 8, but calculation performed with an enhanced $L=0$ component in the wave function. Results shown are for constructive interference ($c_0/c_2 = +0.21$, solid curves) and for destructive interference ($c_0/c_2 = -0.21$, dashed curves) between $L=0$ and 2.

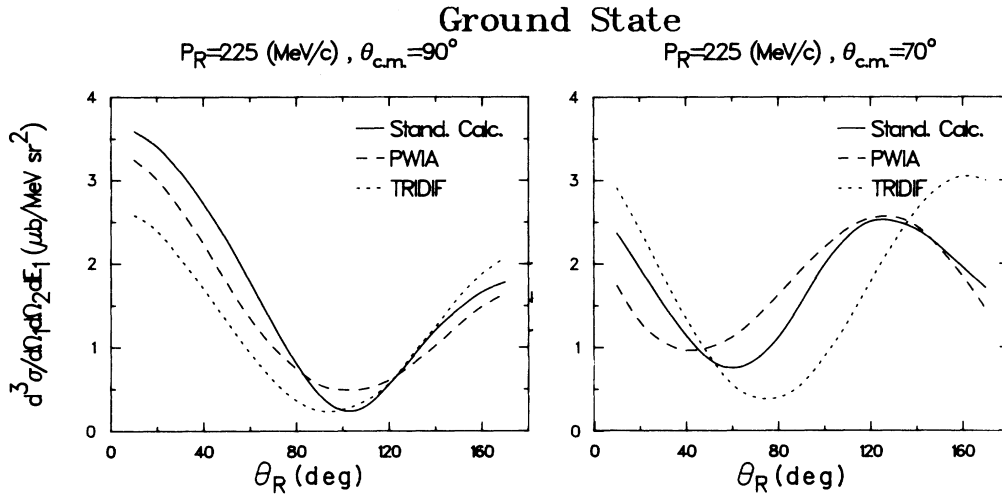


FIG. 10. Same as Fig. 7, but for the transition to the ground state. The results of the calculation have been divided by 2 here in order to facilitate comparison to the TRIDIF results.

ous case.

In view of the qualitative failure documented in Fig. 8, there is a definite chance that the agreement with the θ_R distributions in Fig. 10 is fortuitous. With one single $L \neq 0$ transition available, it is difficult to rule out this possibility. However, it would be rather easy to test our tentative explanation of the recoil angle dependence by measuring other $L \neq 0$ transitions as well, e.g., the 2^+ (7.0 MeV) and 3^+ (11.0 MeV) states in ^{14}N . The QDM predicts strong and characteristic θ_R dependences for these transitions, under similar kinematics [see Eq. (2.23)]. At $\theta_{c.m.} = 90^\circ$, for instance, our analytical formula yields

$$g(\theta_R) \sim \begin{cases} 1 + 3 \cos^2 \theta_R, & [1^+, L=2] \\ 1 - \cos^2 \theta_R, & [2^+] \\ 1 + \frac{1}{2} \cos^2 \theta_R, & [3^+]. \end{cases} \quad (4.3)$$

The behavior is so different that even a rough measurement should allow testing of these predictions. In order to give an idea of the expected cross sections, we have performed DWIA calculations for the 2^+ and 3^+ states, for the same kinematics as in Figs. 5 and 8. The results are shown in Figs. 11 and 12. Notice the difference in shape between the cross sections for the 2^+ and 3^+ transitions,

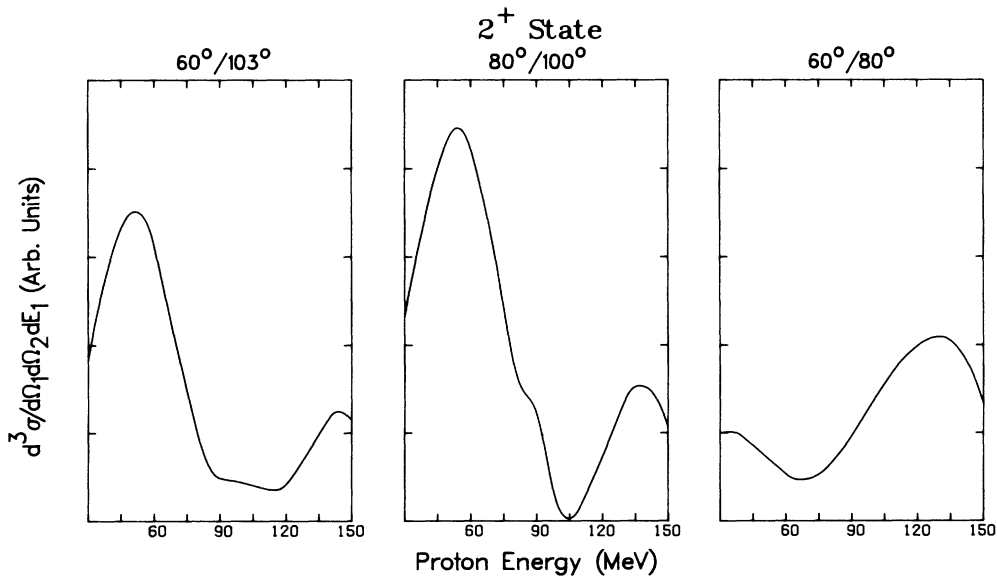


FIG. 11. Results of our standard calculation for the transition to the 2^+ (7.0 MeV) state, at three pairs of detector angles. If we normalize the calculation to the 1^+ (3.9 MeV) state, each section of the vertical axis corresponds to $1.84 \mu\text{b}/\text{sr}^2$.

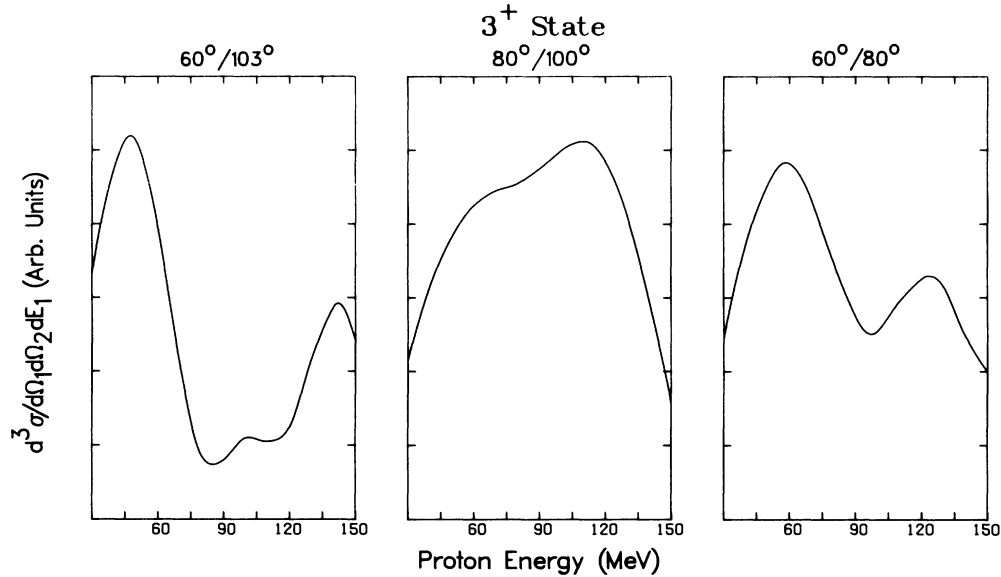


FIG. 12. Same as Fig. 11, but transition to the $3^+(11.0 \text{ MeV})$ state. The same remark about the absolute normalization applies here.

which is exclusively due to the aforementioned polarization effects. Experimental data for transitions different from the 1^+ states studied in Ref. 8 would greatly help disentangle nuclear structure uncertainties from reaction mechanism uncertainties and hopefully shed some light on the problems encountered with the g.s. transition.

V. CONCLUSION

We have recently proposed a phenomenological version of the QDM for low energy pion absorption. The present paper contains the first application of our model to pions in flight. Our test case is the reaction $^{16}\text{O}(\pi^+, pp)^{14}\text{N}$ to definite final states, as measured at LAMPF with 60 MeV pions and high resolution.

Being dominated by $L=0$ transfer, the transition to the 3.9 MeV 1^+ state is expected to have rather simple features. This is indeed borne out by the calculations which reproduce the main characteristics of the data with only one adjustable parameter, the strength of the dominant $\pi\text{NN}\rightarrow\text{NN}$ absorption amplitude ($^3S_1\rightarrow^1D_2$). As compared to stopped pions, it is pleasing to see a greater sensitivity to details of the absorption operator (e.g., finite size effects), owing to the increased number of kinematical variables. The recoil angle dependence at $P_R > 100 \text{ MeV}/c$ observed experimentally and essentially absent in a PWIA can be accounted for very well by distortion effects in the initial and final states. This reminds us that the asymptotic momenta are not identical to the variables defining the elementary absorption process. The sensitivity to the distortion effects is enhanced here, because one is already in the tail of the quasi-free peak.

For the ground state transition the picture is unfortunately much less coherent. Because of the strong $L=2$ component, one certainly expects additional complica-

tions, but the data seem to indicate that some important dynamics is still missing in our model. There is a suggestion of two competing mechanisms, one at low and the other at high recoil momenta. Attempts to attribute the excess cross section near $P_R=0$ to a significant $L=0$ component in the deuteron c.m. wave function failed to reproduce the shape of the measured distributions. As is also evident from the TRIDIF parametrization, one needs a strong, simultaneous dependence on P_R and θ_R , perhaps as a result of some interference. In view of these difficulties, it is surprising that the recoil angle dependence at $P_R \gtrsim 150 \text{ MeV}/c$ is entirely consistent with the prediction of the QDM for an $L=2, 1^+$ state, using the dominant amplitude A_5 only. Our analytical model allows us to attribute this strong θ_R dependence to a (tensor) polarization effect, and the DWIA calculations confirm this interpretation. If our explanation is correct, one should see dramatic and characteristic anisotropies in the recoil angle distributions for the 2^+ and 3^+ states as well. Independently of the outcome of such a comparison, it is necessary to take into account these polarization effects, which are a simple and straightforward consequence of the QDM for 3S_1 pairs. They invalidate a factorization of the cross section into an (unpolarized) elementary $\pi d\rightarrow pp$ cross section, times a distorted momentum distribution, which has sometimes been used in this context. Experimental data for other transitions with $L\neq 0$ (e.g., $2^+, 3^+$) would be extremely valuable, both to verify systematically the presence of polarization effects and to help eliminate nuclear structure uncertainties.

This work has been supported by the "Stichting voor Fundamenteel Onderzoek der Materie (FOM)," which is financially supported by the "Nederlandse Organisatie voor Zuiver Wetenschappelijk Onderzoek (ZWO)."

APPENDIX: GENERALIZATION
OF THE EFFECTIVE DENSITY MATRIX

For a 1^+ transition with contributions from $L=0$ (c_0) and $L=2$ (c_2) transfer, Eq. (2.9) of I for the effective density matrix of the "quasi-deuteron" has to be replaced by

$$\begin{aligned} \rho_i^{\text{eff}} = N(P) \sum_M (c_0 R_0 \langle \hat{\mathbf{P}} | 011M \rangle + c_2 R_2 \langle \hat{\mathbf{P}} | 211M \rangle) \\ \times (c_0 R_0 \langle 011M | \hat{\mathbf{P}} \rangle + c_2 R_2 \langle 211M | \hat{\mathbf{P}} \rangle). \end{aligned} \quad (\text{A1})$$

The normalization factor $N(P)$ can be determined from $\text{Tr} \rho_i^{\text{eff}} = 1$, but is not needed here. The R_L stand for $R_L^{(0101)}(P)$; cf. Appendix 2 of I. The M sum in (A1) can be performed as follows:

$$\begin{aligned} \sum_M \langle \hat{\mathbf{P}} | 011M \rangle \langle 011M | \hat{\mathbf{P}} \rangle &= \frac{1}{4\pi}, \\ \sum_M \langle \hat{\mathbf{P}} | 211M \rangle \langle 211M | \hat{\mathbf{P}} \rangle \\ &= \frac{1}{4\pi} \left[1 - \left(\frac{2\pi}{5} \right)^{1/2} Y_2(\hat{\mathbf{P}}) \cdot \tau_2 \right], \end{aligned} \quad (\text{A2})$$

$$2 \text{Re} \sum_M \langle \hat{\mathbf{P}} | 011M \rangle \langle 211M | \hat{\mathbf{P}} \rangle = \frac{1}{\sqrt{5}\pi} Y_2(\hat{\mathbf{P}}) \cdot \tau_2.$$

Consequently, we get

$$\begin{aligned} \rho_i^{\text{eff}} = \frac{N(P)}{4\pi\sqrt{10}} [\sqrt{10}(c_0^2 R_0^2 + c_2^2 R_2^2) \\ + \sqrt{4\pi}(\sqrt{8}c_0 c_2 R_0 R_2 - c_2^2 R_2^2) Y_2(\hat{\mathbf{P}}) \cdot \tau_2]. \end{aligned} \quad (\text{A3})$$

Upon comparing this with the general expression (2.19), we arrive at the desired result, Eq. (3.11).

- ¹D. Ashery and J. P. Schiffer, *Annu. Rev. Nucl. Part. Sci.* (in press).
²J. Favier *et al.*, *Nucl. Phys.* **A169**, 540 (1971).
³E. D. Arthur *et al.*, *Phys. Rev. C* **11**, 332 (1975).
⁴B. Bassalleck *et al.*, *Phys. Rev. C* **16**, 1526 (1977).
⁵B. Bassalleck *et al.*, *Nucl. Phys.* **A343**, 365 (1980).
⁶H. P. Isaak *et al.*, *Helv. Phys. Acta* **55**, 477 (1982).
⁷P. Heusi *et al.*, *Nucl. Phys.* **A407**, 429 (1983).
⁸W. R. Wharton *et al.*, *Phys. Rev. C* **31**, 526 (1985).
⁹R. Rieder *et al.*, *Phys. Rev. C* **33**, 614 (1986).
¹⁰M. Gouweloos and M. Thies, *Nucl. Phys.* **A455**, 602 (1986).
¹¹C. Richard-Serre *et al.*, *Nucl. Phys.* **B20**, 413 (1970).
¹²C. M. Rose, *Phys. Rev.* **154**, 1305 (1967).
¹³K. Aniol *et al.*, *Phys. Rev. C* **33**, 1714 (1986).

- ¹⁴I. Navon *et al.*, *Phys. Rev. C* **28**, 2548 (1983).
¹⁵K. Stricker, H. McManus, and J. A. Carr, *Phys. Rev. C* **19**, 929 (1979).
¹⁶B. G. Ritchie *et al.*, *Phys. Rev. C* **27**, 1685 (1983).
¹⁷S. Cohen and D. Kurath, *Nucl. Phys.* **A141**, 145 (1970).
¹⁸A. van der Woude and R. J. Meijer, *Nucl. Phys.* **A258**, 199 (1976).
¹⁹T.-S. H. Lee, K. Ohta, and M. Thies, *Ann. Phys. (N.Y.)* **163**, 420 (1985).
²⁰C. A. Engelbrecht and H. Fiedeldey, *Ann. Phys. (N.Y.)* **12**, 262 (1967).
²¹M. Gouweloos, Ph.D. thesis, Free University of Amsterdam, 1986.